DOI: 10.61782/fa.2025.0755

FORUM ACUSTICUM EURONOISE 2025

ROBUST SPATIOTEMPORAL WAVE LOCALIZATION IN PIEZOELECTRIC METAMATERIALS THROUGH PROGRAMMABLE TOPOLOGICAL INTERFACE STATES

Bruno Alceu Souto [1*] **Danilo Beli** [2] **Carlos De Marqui Jr**[1]

[1] Department of Aeronautical Engineering, University of Sao Paulo, Brazil
[2] Department of Mechanical Engineering, Eindhoven University of Technology, the Netherlands

ABSTRACT

The emergence of topological states in condensed matter physics has provided reliable mechanisms for waveguiding in phononic crystals and metamaterials. This study introduces a strategy for dynamic wave localization using space-time programmable topological interface states in piezoelectric metamaterials. By dynamically tuning inductive shunt circuits, we induce and modulate interface states in space and time without physical changes in the host structure. By modulating electrical properties, the topological interface can be dynamically moved along the beam, enabling efficient energy transfer. The numerical results clarify the effects of modulation smoothness on wave localization for cases with and without structural damping, identifying the optimal conditions for robust energy transfer.

Keywords: *piezoelectricity, programmable metamaterial, topological interface states, structural damping*

1. INTRODUCTION

The discovery of topological states in condensed matter physics has led to innovative methods for manipulating waves in metamaterials [1, 2]. The topological protection of these states, which confine mechanical waves to edges or interfaces between regions with distinct topological properties [3], provides robustness against backscattering caused by imperfections or disturbances along the propagation path [4]. In contrast to their electronic counterparts [5], acoustic and elastic systems offer greater flexibility in the design, fabrication, and detection of diverse topological phenomena [6]. In this context, breaking the spatial inversion symmetry while maintaining the time-reversal symmetry can be achieved in the subwavelength regime by manipulating piezoelectric inductive shunt circuits [7]. In this sense, connecting two metamaterials with distinct Zak phases allows the emergence of a topological interface state that presents significant vibration energy localization [8].

Recent years have seen significant interest in exploring metamaterials with adaptable and programmable characteristics, particularly due to their potential for versatile control over wave propagation. [9]. Recent studies have concentrated on multi-coupling domains to improve reconfigurability. Within this context, piezoelectric materials have become a popular choice due to their versatility in controlling wave behavior. This is achieved by adjusting digitally controlled analog and digital shunt circuits, as opposed to traditional analog shunts. This advancement has enabled the experimental implementation of programmable metamaterials [10, 11]. This advanced control strategy enables the design of materials with spatiotemporal modulation, enhancing metamaterials by adding an extra dimension of tunability through dynamic adjustments of their properties in both space and time [12].

In this work, we build upon a recently introduced approach that utilizes space-time modulation of trivial de-

*Corresponding author: brunoalceu@usp.br.

fects [13, 14] and extend it to programmable topological interfaces within an electromechanically coupled metamaterial beam. By applying cosine-based modulations to the electrical properties of the unit cells, we demonstrate that the topological interface can be dynamically repositioned along the beam, enabling efficient energy transfer while preventing energy leakage. Additionally, we discuss the effects of structural damping on the modulation performance and energy availability for further operations.

2. MODEL DESCRIPTION

Fig. 1 depicts the electromechanical metamaterial, which consists of a thin conductive substructure sandwiched by two oppositely poled piezoelectric layers. The outer surfaces of the thin and conductive electrodes covering each piezoelectric layer are periodically segmented, and each segment is connected to an inductive shunt circuit, characterizing a local resonator with the equivalent in-series piezoelectric capacitance. The unit cell highlighted in Fig. 1 comprises four consecutive local resonators with the outer and inner inductances set as L_1 (blue inductances) and L_2 (red inductances), respectively. Thus, the unit cell has a mirror symmetry regarding the central point. A dimerization parameter δ is defined to generate $L_1 = L_r(1+\delta)$ and $L_2 = L_r(1-\delta)$, where L_r is a reference inductance.

The metamaterial beam is discretized into one-dimensional finite elements based on the Euler-Bernoulli assumptions. A third-degree polynomial is employed to approximate the transverse displacement field within each element that has two degrees of freedom per node, denoted as transverse displacement (w) and rotation about the y direction (θ) [15]. In the electrical domain, the non-zero electric field component is assumed to be uniform in the thickness direction of the piezoelectric layers. Consequently, one electrical degree of freedom is sufficient to model the voltage output in each electrode's segment. The structural dissipation is included using Rayleigh's proportional damping model. Consequently, the behavior of the piezoelectric metamaterial beam is governed by the following finite elements equations [16],

$$\mathbf{M}\ddot{\mathbf{u}} + \mathbf{D}\dot{\mathbf{u}} + \mathbf{K}\mathbf{u} - \boldsymbol{\Theta}\mathbf{v} = \mathbf{F} \tag{1a}$$

$$\mathbf{C_p}\mathbf{v} + \mathbf{q} + \boldsymbol{\Theta}^t\mathbf{u} = \mathbf{0} \tag{1b}$$

where $\mathbf{M}$ is the global mass matrix ($n_m \times n_m$), $\mathbf{K}$ is the global stiffness matrix ($n_m \times n_m$), $\mathbf{D}$ is the structural damping matrix ($n_m \times n_m$), $\mathbf{F}$ is the vector of external mechanical inputs ($n_m \times 1$), $\boldsymbol{\Theta}$ is the electromechanical coupling matrix ($n_m \times n_e$), $\mathbf{C_p}$ is the capacitance matrix ($n_m \times n_e$), $\mathbf{v}$ is the vector of voltage output from each electrode segment ($n_e \times 1$), $\mathbf{q}$ is the vector of electrical charges ($n_e \times 1$), $\mathbf{u}$ is the vector of mechanical degrees of freedom ($n_m \times 1$), which contains the transverse displacements and rotations (about the y direction) associated to each node, and n_m and n_e are the number of mechanical and electrical degrees of freedom, respectively. The over-dots represent the derivative with respect to time t.

When considering time-varying inductances in each shunt circuit, the voltage output from each electrode segment is determined by $\mathbf{v}(t) = \dot{\mathbf{L}}_c(t)\dot{\mathbf{q}} + \mathbf{L_c}(t)\ddot{\mathbf{q}}$, where $\mathbf{L_c}$ is a diagonal matrix ($n_e \times n_e$) that contains the inductances connected to each segment of electrode. In this case, the matrix representation of Eqs. 1 is

$$\begin{bmatrix} \mathbf{M} & -\boldsymbol{\Theta}\mathbf{L_c} \\ \mathbf{0} & \mathbf{C_p}\mathbf{L_c} \end{bmatrix} \begin{bmatrix} \ddot{\mathbf{u}} \\ \ddot{\mathbf{q}} \end{bmatrix} + \begin{bmatrix} \mathbf{D} & -\boldsymbol{\Theta}\dot{\mathbf{L}}_\mathbf{c} \\ \mathbf{0} & \mathbf{C_p}\dot{\mathbf{L}}_\mathbf{c} \end{bmatrix} \begin{bmatrix} \dot{\mathbf{u}} \\ \dot{\mathbf{q}} \end{bmatrix} + \begin{bmatrix} \mathbf{K} & \mathbf{0} \\ \boldsymbol{\Theta}^t & \mathbf{I} \end{bmatrix} \begin{bmatrix} \mathbf{u} \\ \mathbf{q} \end{bmatrix} = \begin{bmatrix} \mathbf{F} \\ \mathbf{0} \end{bmatrix} \tag{2}$$

where $\mathbf{I}$ is the identity matrix ($n_e \times n_e$). Equation 2 represents a multiphysical problem, wherein the mechanical and electrical domains are coupled through the electromechanical coupling matrix $\boldsymbol{\Theta}$ (off-diagonal elements of the matrices). In each unit cell, the combination of the inductive shunt L_{c_j} and the effective capacitance of the piezoelectric bimorph C_{p_j} forms a capacitive-inductive circuit whose resonance frequency is $\omega_{n_j} = 1/\sqrt{C_{p_j} L_{c_j}}$.

In Fig. 1, each electrode segment has length l_s and width b equal to 20 mm. The substructure has thickness h_s of 1 mm, the elastic modulus is $c_s = 69$ GPa, and mass density $\rho_s = 2700\,\mathrm{kg/m^3}$. The substructure is sandwiched by two PMN-PT piezoelectric layers, each with a thickness h_p of 0.6 mm. The elastic modulus of the PMN-PT crystal at a constant electric field is $\bar{c}_{11}^E$ of 21.8GPa, an effective piezoelectric stress constant $\bar{e}_{31}$ of $-14.1\,\mathrm{C/m^2}$, a permittivity component at a constant strain $\bar{\epsilon}_{33}^S$ of 33 nF/m, and a mass density ρ_p of $8120\,\mathrm{kg/m^3}$.

The angular frequency axis in the results is normalized by the velocity of the longitudinal wave considering the composite material's average properties. Accordingly, the normalized frequency assumes $\Omega = \omega l_s/(2\pi\sqrt{Y_{avg}\rho_{avg}})$, where $Y_{avg} = v_f/Y_s + (1-v_f)/Y_p$ and $\rho_{avg} = v_f\rho_s + (1-v_f)\rho_p$ are the average modulus and the average mass density, respectively, while

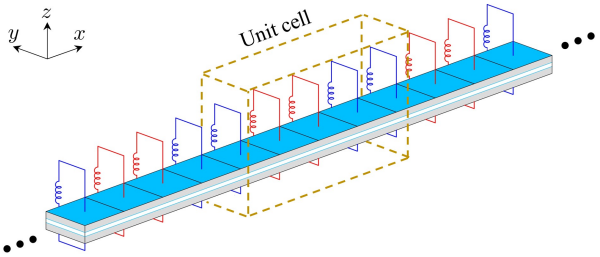

Figure 1. Scheme of the locally resonant electromechanical metamaterial, where the light gray and white regions represent the piezoelectric and substructure layers, the blue regions represent the electrodes. The highlighted region depicts the unit cell, where the blue and red inductances are associated with L_1 and L_2, respectively.

$v_f = h_s/(h_s + 2h_p)$ is the volume fraction of the substructure and $Y_p = 1/s_{11}^E$ is the piezoelectric elastic modulus. In addition, the finite element mesh for the numerical calculations is assumed as 12 elements per unit cell, which gives approximately 1.1 mm for each element. This value corresponds to 3% of the smallest wavelength analyzed, which can capture the studied dynamic behavior effectively.

3. RESULTS

Fig. 2 depicts the band structure for three unit cells, one tuned with $\delta = 0$ (Fig. 2(a)) and tuned with $\delta = \pm 0.05$ (Fig. 2(b)), where $L_r = 0.576$ H. The unit cells tuned with $\delta = 0.05$ are named UCA in this work while the ones tuned with $\delta = -0.05$ are UCB. The numerical procedures combine the Bloch-Floquet periodic conditions with the finite element matrices where the electrical outputs are considered internal degrees of freedom (for more details, see [13]). An inverse eigenproblem (i.e., $\omega(\kappa)$) is solved for each wavenumber κ. According to the presented results, the homogeneous unit cell (i.e., $\delta = 0$) features a locally resonant band gap between $\Omega_l = 0.0153$ and $\Omega_u = 0.0169$. In addition, a folding point appears at $\Omega_f = 0.0150$ (red circle in Fig. 2(a)). The folding point opens to generate a band gap in the subwavelength region (green region) for the non-homogeneous unit cell (i.e., $\delta \neq 0$). Although the band structures of the unit cells tuned with $\delta \pm 0.05$ are identical, they have distinct topological properties due to band transition and inversion, which characterizes a topologically non-trivial band gap [17].

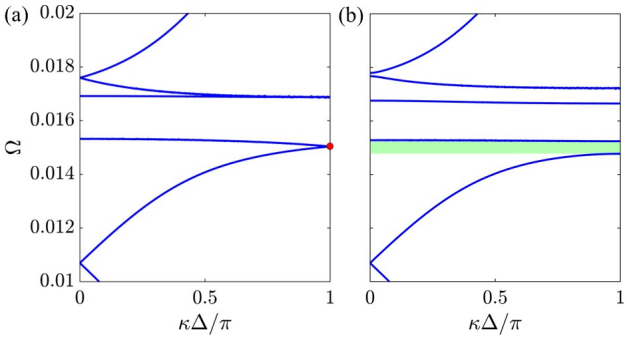

Figure 2. Dispersion relation of the unit cell tuned with $\delta = 0$ (a) and $\delta = \pm 0.05$. The red circle indicates the folding point whereas the green region highlights the non-trivial band gap.

The emergence of a topological interface mode is examined through the harmonic response of a finite piezoelectric metamaterial beam consisting of 16 unit cells — 8 unit cells UCA to the right and 8 unit cells UCB to the left, creating an interface between them. A harmonic point excitation, denoted as $\bar{F}(L/2, \Omega)$ (where L represents the total length of the metastructure), is applied at the interface position. The corresponding harmonic transverse displacements, $\bar{w}(x, \Omega)$, are obtained along the metastructure as well as the amplitude of the transfer functions $20\log_{10}|\hat{w}(x, \Omega)/\hat{F}|$ (dB, reference 1 m/N). Fig. 3(a) shows the harmonic response as a function of space and frequency for the periodic configuration (the metamaterial beam with 16 unit cells tuned with $\delta = 0.05$). Fig. 3(b) displays the harmonic response for the topological metamaterial (metamaterial with 8 unit cells tuned with $\delta = 0.05$ and 8 unit cells tuned with $\delta = -0.05$). Three attenuation zones are observed in the responses of the periodic configuration and the topological metamaterial beam. These consist of two Bragg band gaps and a locally resonant band gap situated between them, which is consistent with the dispersion previously presented for the unit cells. Figure 3(b) displays a resonance peak within the first non-trivial Bragg band gap (green region depicted in Fig. 2(b)), which corresponds to the topological interface state.

After examining the behavior of a topological metamaterial with a fixed interface, we now investigate its pro-

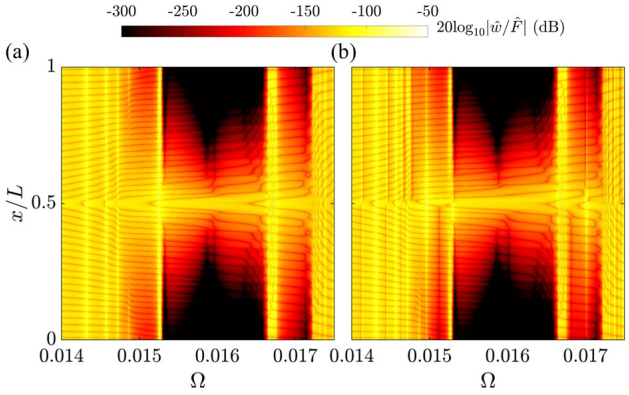

Figure 3. Maps displaying harmonic responses as a function of both spatial position and frequency for the periodic metastructure without topological interface (a) and for the topological metastructure with topological interface (b).

grammable counterpart. We perform the space-time wave localization by dynamically modulating the interface in both space and time. This approach involves transforming one of the unit cells adjacent to the interface into its topological counterpart while keeping the others unchanged. As a result, the interface can only shift between successive unit cell boundaries within a single modulation cycle. In this framework, modifying a unit cell initially set to $\delta = 0.05$ ($\delta = -0.05$) requires that the inner electromechanical resonators are changed from Ω_{t_1} (Ω_{t_2}) to Ω_{t_2} (Ω_{t_1}), while simultaneously updating the outer electromechanical resonators from Ω_{t_2} (Ω_{t_1}) to Ω_{t_1} (Ω_{t_2}). Consequently, vibrational energy is expected to be transferred from the initial interface location to the final interface position.

The essential mechanism for achieving a perfect energy transfer across successive unit cell boundaries involves the smooth and synchronized adjustment of each local resonator's frequency. In this study, cosine functions are employed to modulate the local resonant frequency, affecting the inductance of each shunt circuit during space-time transitions. These functions are of interest in this application since they present zero-time derivatives at the beginning and end of the transition intervals and are continuous throughout the entire domain. For convenience, we denote the unit cells on the left and right of the topological interface with the indices j and $j+1$, respectively. If the interface is intended to move to the right (left) side, then the unit cell represented by $m = j+1$ ($m = j$) is topologically converted. Furthermore, consider Ω_{m_1} and Ω_{m_2} as the frequencies of local resonators, which are initially tuned to Ω_{t_1} and Ω_{t_2} within the unit cell m to be converted, respectively. Therefore, the variation of the locally resonant frequencies defined by Ω_{m_1} from $\Omega_{m_1}/\Omega_{t_1} = 1$ to $\Omega_{m_1}/\Omega_{t_1} = \Omega_{t_2}/\Omega_{t_1} = \eta$ is governed by the following law during the time interval $t_{i_j} \leq t \leq t_{f_j}$:

$$\frac{\Omega_{m_1}}{\Omega_{t_1}}(t) = \frac{(1+\eta)}{2} - \frac{(\eta-1)}{2}\cos\left(\frac{t-t_{i_j}}{t_{f_j}-t_{i_j}}\pi\right) \quad (3)$$

simultaneously, the change in locally resonant frequencies defined by Ω_{m_2} from $\Omega_{m_2}/\Omega_{t_1} = \eta$ to $\Omega_{m_2}/\Omega_{t_1} = 1$:

$$\frac{\Omega_{m_2}}{\Omega_{t_1}}(t) = \frac{(1+\eta)}{2} + \frac{(\eta-1)}{2}\cos\left(\frac{t-t_{i_j}}{t_{f_j}-t_{i_j}}\pi\right) \quad (4)$$

where t_{i_j} and t_{f_j} are, respectively, the initial and final time steps of the transition. Likewise, the transition about the mth unit cell can be characterized through $\delta_m(t) = (\Omega_{m_2}(t)^2 - \Omega_{m_1}(t)^2)/(\Omega_{m_2}(t)^2 + \Omega_{m_1}(t)^2)$. The rate of change of the frequencies of the local resonator, $d\Omega_{m_1}/dt$ and $d\Omega_{m_2}/dt$, affects the energy transfer over space and time. To control the transition smoothness, we define the transition interval as integer multiples N_j of the excitation period T, i.e., $\Delta\tau_j = t_{f_j} - t_{i_j} = N_j T$. In the case involving more unit cells, e.g., the interface displacement from the boundary between the jth and $(j+1)$th unit cells to the boundary between the $(j+3)$th and $(j+4)$th unit cells, the time values must be chosen so that $t_{i_{j+2}} \geq t_{f_{j+1}}$ and $t_{i_{j+3}} \geq t_{f_{j+2}}$, which means that the next transition only begins when the previous has been finished.

The feasibility of the previously discussed strategy is illustrated through simulations in the time domain. The Newmark method at a constant time step configured with $\gamma = 0.5$ and $\beta = 0.25$ (average constant acceleration scheme) [18] was employed to conceive multiple transition scenarios. A point force excitation is applied at the interface position and modeled as a sine burst (sinusoidal envelope) with a central frequency of $\Omega = 0.01496$ (corresponding to the frequency of the topological interface mode). The force magnitude is 0.1 N with a duration of 100 periods (i.e., $100T$, where T corresponds to one period). The interface is initially assumed at the center of the beam, between unit cells 8 and 9. Equations 3 and 4 are used to create the programmable topological interface from the center of the beam to the location between unit cells 12 and 13.

In the first transition unit cell 9 is changed from $\delta = -0.05$ to $\delta = 0.05$, i.e., the inductors are time modulated from the $L_2L_1L_1L_2$ configuration to $L_1L_2L_2L_1$ and, therefore, the space-time vibration energy localization around the new interface position (between unit cells 9 and 10) is observed. Subsequently, unit cell 10 is modified from $\delta = -0.05$ to $\delta = 0.05$ configuration, resulting in space-time vibration energy localization around the new interface position between unit cells 10 and 11. Later, the electrical inductances of the unit cell 11 are updated, resulting in the new tuning $\delta = 0.05$ and, consequently, changing the interface to the new position between unit cells 11 and 12. Finally, unit cell 12 is gradually changed from $\delta = -0.05$ to $\delta = 0.05$, creating a new interface between unit cells 12 and 13 and, finally, vibration energy localization around the new topological interface position.

Fig. 4 displays the transitions for two cases. The first one, displayed in Fig. 4(a), assumes an undamped configuration and $N = 100$. The white dots delimit the modulation intervals, where the stages II to V represent the time modulation of the inductors of unit cells 9 to 12, respectively. The perfect space-time vibration energy transfer along each smooth transition is observed in Fig. 4(a), where the energy initially confined around the center of the metamaterial beam is gradually and perfectly transferred to the final interface position. Fig. 4(b) shows the result for a damped configuration, i.e., $\zeta = 0.002$. Even considering that the amplitude of motion is reduced over time due to dissipation effects, vibration energy is localized at the final interface position. Although not shown in this work, there is a trade-off between modulation speed and the available energy in the final state in the presence of damping [14].

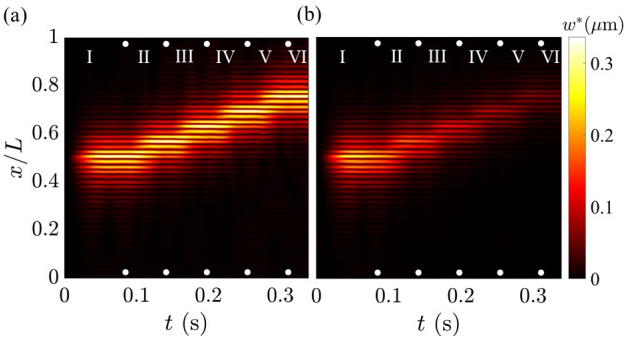

Figure 4. Multiple smooth modulations for the undamped (a) and damped (b) cases.

4. CONCLUSIONS

This study introduced a framework for space-time wave localization using programmable topological interface states in electromechanically coupled metamaterials. Energy transfer between programmable interfaces was successfully demonstrated by smoothly modulating inductive shunt circuits in an undamped metastructure. Although the amount of vibration energy was reduced throughout the modulations, successful modulations could be observed in the presence of structural damping.

5. ACKNOWLEDGMENTS

The authors are grateful to the National Council for Scientific and Technological Development grant # 383782/2022-8 and to the São Paulo Research Foundation grants # 2018/18774-6, # 21/12700-3 and # 2018/15894-0.

6. REFERENCES

[1] G. Ma, M. Xiao, and C. T. Chan, "Topological phases in acoustic and mechanical systems," *Nature Reviews Physics*, vol. 1, pp. 281–294, Apr 2019.

[2] W. Zhu, W. Deng, Y. Liu, J. Lu, H.-X. Wang, Z.-K. Lin, X. Huang, J.-H. Jiang, and Z. Liu, "Topological phononic metamaterials," *Reports on Progress in Physics*, vol. 86, p. 106501, sep 2023.

[3] R. K. Pal and M. Ruzzene, "Edge waves in plates with resonators: an elastic analogue of the quantum valley hall effect," *New Journal of Physics*, vol. 19, p. 025001, feb 2017.

[4] Y. Jin, D. Torrent, and B. Djafari-Rouhani, "Robustness of conventional and topologically protected edge states in phononic crystal plates," *Phys. Rev. B*, vol. 98, p. 054307, Aug 2018.

[5] M. Z. Hasan and C. L. Kane, "Colloquium: Topological insulators," *Rev. Mod. Phys.*, vol. 82, pp. 3045–3067, Nov 2010.

[6] H. Huang, J. Chen, and S. Huo, "Recent advances in topological elastic metamaterials," *Journal of Physics: Condensed Matter*, vol. 33, p. 503002, oct 2021.

[7] Z. Wu, R. Xia, J. Yi, and Z. Li, "Multiple topological interface modes in electromechanically resonant piezoelectric beams," *Engineering Structures*, vol. 281, p. 115716, 2023.

[8] Y. Liu, H. Wang, W. Fang, Q. Han, D. Liu, and Y. Liang, "Tunable control of subwavelength topological interface modes in locally resonance piezoelectric metamaterials," *Composite Structures*, vol. 276, p. 114541, 2021.

[9] Y.-F. Wang, Y.-Z. Wang, B. Wu, W. Chen, and Y.-S. Wang, "Tunable and Active Phononic Crystals and Metamaterials," *Applied Mechanics Reviews*, vol. 72, 02 2020. 040801.

[10] C. Sugino, M. Ruzzene, and A. Erturk, "Digitally programmable resonant elastic metamaterials," *Phys. Rev. Appl.*, vol. 13, p. 061001, Jun 2020.

[11] T. M. P. Silva, M. A. Clementino, V. C. de Sousa, and C. De Marqui, "An experimental study of a piezoelectric metastructure with adaptive resonant shunt circuits," *IEEE/ASME Transactions on Mechatronics*, vol. 25, no. 2, pp. 1076–1083, 2020.

[12] J. Santini and E. Riva, "Elastic temporal waveguiding," *New Journal of Physics*, vol. 25, p. 013031, feb 2023.

[13] R. L. Thomes, D. Beli, and C. De Marqui, "Space–time wave localization in electromechanical metamaterial beams with programmable defects," *Mechanical Systems and Signal Processing*, vol. 167, p. 108550, 2022.

[14] R. L. Thomes, D. Beli, C. Sugino, A. Erturk, and C. D. M. Junior, "Programmable moving defect for spatiotemporal wave localization in piezoelectric metamaterials," *Phys. Rev. Appl.*, vol. 19, p. 064031, Jun 2023.

[15] M. Petyt, *Introduction to Finite Element Vibration Analysis*. Cambridge University Press, 1998.

[16] C. De Marqui Junior, A. Erturk, and D. J. Inman, "An electromechanical finite element model for piezoelectric energy harvester plates," *Journal of Sound and Vibration*, vol. 327, no. 1, pp. 9–25, 2009.

[17] M. Xiao, Z. Q. Zhang, and C. T. Chan, "Surface impedance and bulk band geometric phases in one-dimensional systems," *Phys. Rev. X*, vol. 4, p. 021017, Apr 2014.

[18] N. M. Newmark, "A method of computation for structural dynamics," *Journal of the Engineering Mechanics Division*, vol. 85, no. 3, pp. 67–94, 1959.